



# Optical attenuation coefficient of skin under low compression

RAQUEL PANTOJO DE SOUZA BACHOUR,<sup>1</sup> CHRISTIAN TOLENTINO DOMINGUEZ,<sup>2,\*</sup> AND GEORGE C. CARDOSO<sup>1</sup>

<sup>1</sup>Physics Department FFCLRP, University of São Paulo, Ribeirão Preto, SP 14040-901, Brazil

<sup>2</sup>Physics Department CCEN, Universidade Federal da Paraíba, João Pessoa, PB 58051-900, Brazil

\*christian@opto.cetuc.puc-rio.br

Received 5 December 2022; revised 29 March 2023; accepted 29 March 2023; posted 29 March 2023; published 20 April 2023

In various biomedical optics therapies, knowledge of how light is absorbed or scattered by tissues is crucial. Currently, it is suspected that a low compression applied to the skin surface may improve light delivery into tissue. However, the minimum pressure needed to be applied to significantly increase the light penetration into the skin has not been determined. In this study, we used optical coherence tomography (OCT) to measure the optical attenuation coefficient of the human forearm dermis in a low compression regime (<8 kPa). Our results show low pressures such as 4 kPa to 8 kPa are sufficient to significantly increase light penetration by decreasing the attenuation coefficient by at least 1.0 mm<sup>-1</sup>. © 2023 Optica Publishing Group

<https://doi.org/10.1364/JOSAA.482664>

## 1. INTRODUCTION

The optical attenuation coefficient ( $\mu_t$ ) measures how light is attenuated as it passes through a medium. The knowledge of  $\mu_t$  helps us to understand light–matter interaction. In homogeneous media, optical attenuation comprises absorption and scattering [1], described independently by the absorption coefficient ( $\mu_a$ ) and the scattering coefficient ( $\mu_s$ ), respectively.

The optical properties of tissues are of great interest in optical diagnostics and light-based therapies and treatments [2]. In the last decades, light has become an important diagnostic tool in many medical fields, such as ophthalmology and dermatology [3], and more recently started to be used in non-invasive blood glucose monitoring [4,5]. An example of a treatment tool is photodynamic therapy, which uses light to excite a particular chromophore to perform energy transitions and chemical reactions capable of damaging cells and eliminating microorganisms [6,7]. It should be noted that the optical attenuation, which includes both scattering and absorption, depends on the spectral properties of the light interacting with the living tissue [8].

Skin compression modifies the spatial distribution of light within the tissue and may improve light penetration. Compression changes the tissue layer thickness and the volumetric fraction of components such as water, proteins, and lipids influencing light transport, with specific spectral dependencies [9,10]. Rylander *et al.* [9] suggested that the use of mechanical compression has the potential to improve light delivery for emerging optical and therapeutic imaging applications. They observed that compression caused an increase of 1.5 dB in detected signal intensity. Kirillin *et al.* [10] found similar results, where compression caused an increase in the image contrast

of the epidermal–dermal junction. Su *et al.* [11] suggested compression can be used for clinical diagnostic applications, including monitoring blood glucose non-invasively.

In this study, we investigate *in vivo* changes in the optical attenuation coefficient of skin at low compressions (<8 kPa). We use optical coherence tomography (OCT) at 1300 nm to acquire images of the human forearm with or without compression on the skin surface. The single scattering model [12,13] was used for regression on the acquired OCT depth profile experimental images. From the regression, we determined the attenuation coefficient of the first region (first 0.12 mm) of the dermis. Low-compression skin has received limited attention [10]. Our goal was to investigate the presence of windows with a reduced attenuation coefficient at low compression levels. Such windows or regions could potentially facilitate better optical penetration, leading to improved diagnosis and therapies.

## 2. METHOD

### A. Experimental Methodology

The attenuation coefficient can be determined from the slope of an OCT depth profile [14–16]. Further elaboration on this technique will be provided in a subsequent section. We obtained B-scan images using OCT equipment (OCS1300SS, Thorlabs Inc. NY) with a 1300 nm central wavelength, a 100 nm bandwidth, a 16 kHz axial scan rate, and 12 μm and 25 μm axial and lateral resolutions, respectively.

Three healthy volunteers (one female, two males), aged 30 to 50 years old, with skin phototype Fitzpatrick type III–IV, without a history of cardiovascular disease, participated in this

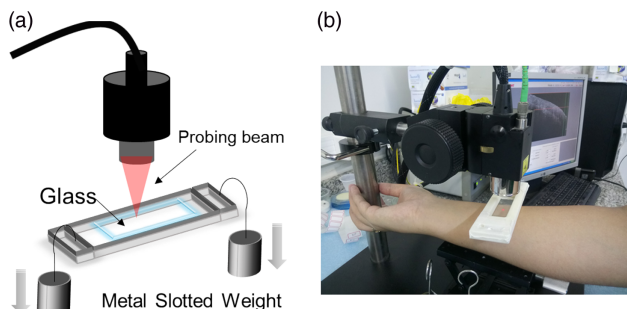


**Fig. 1.** Experimental setup to acquire OCT images of the skin. (a) Homemade 3D-printed support developed to perform compressions. (b) Illustrative photograph of the positioning of the volunteer's forearm during the image acquisition (without weights).

study. The Ethical Committee of the University of São Paulo approved the project, and the volunteers were informed about the procedures. Those who agreed signed a free and informed consent form.

To acquire the OCT images, the volunteers stood with one of their forearms on a horizontal support plate during the scanning, as shown in Fig. 1. Compression was applied over previously selected regions of the volunteer forearm, at approximately 9 cm from the first line of the wrist. For compression, a homemade 3D-printed support was built to hold at its bottom a microscope glass slide (75 mm × 25 mm × 1 mm), which was in direct contact with the skin of the volunteer [Fig. 1(b)]. The total weight of the 3D-printed structure plus microscope slide was 24 g. The OCT probing beam was positioned at the center of the glass slide. For the lowest compression, no slotted weights were used. Compression was varied by attaching slotted metal weights to the 3D-printed support to make the total weight vary from 24 g to 1489 g. When used, the slotted metal weights were positioned symmetrically on the sides of the 3D-printed support [Fig. 1(a)]. The experimental design aimed to ensure a uniform pressure across the glass–skin contact region without affecting the pressure distribution in the central region of the contact area. For compression stabilization, OCT scanning was initiated 160 s after positioning of the glass plate and weights. By choosing a small OCT scanned area positioned at center of the contact areas [120 pixels × 60 pixels (3 mm × 2 mm)], we ensured compression uniformity within the analyzed skin surface.

To determine the applied compression, we measured the skin–glass contact area for each one of the applied compressions. We smeared the glass slide with commercial white toothpaste to observe the contact area with the skin. To prevent measurement bias due to a possible physiological reaction of the skin to the toothpaste, the measurements of the contact areas were performed at the end of all the OCT sessions.

## B. Signal Processing

We divided the signal processing into two steps: (i) depth profile computation and post-processing of OCT images, and (ii) data regression to determine the attenuation coefficient of the superficial layer of the dermis, the papillary dermis [17].

### 1. Step 1: Depth Profile Computation and Post-Processing

We acquired B-scan OCT images consisting of 800 pixels by 512 pixels (width by depth) at a rate of 10 frames per second. A total of 60 B-scans were acquired for each compression. A script written in MATLAB v.2015a (Mathworks, USA) processed the images. The script cropped from the center of each B-scan a region of interest (B-scan ROI) 120 pixels by 512 pixels (width by depth that we define as  $\Delta x$  by  $\Delta z$ ). The sequence of cropped B-scan ROI is shown in Fig. 2(a), where a series of  $z$  versus  $x$  as a function of time can be seen.

The skin surface was defined at the air–skin interface (no compression) or the glass–skin interface (with compression). Each B-scan ROI was averaged in the  $x$  direction. The resulting averages were combined to form the profile ( $z$ ) versus time matrix, where the time dimension comprises 60 A-scan ROIs [Fig. 2(b)]. To detect the skin surface, we applied a 2D Canny edge detector filter [18,19] using the MATLAB function `edge(I, "Canny")` from its Image Processing toolbox. The skin edge is shown in Fig. 2(c). The identified edge [Fig. 2(c)] was used to horizontally realign the skin surface to ensure correction for possible nonuniformities of the skin surface with or without compression [Fig. 2(d)].

The Canny filter detects the maximum gray level of each depth profile [see Fig. 2(c)] that corresponds to the stratum corneum layer and realigns them. The maximum intensity of the stratum corneum layer can be easily detected by the edge detection algorithm because of the high discontinuity in the refraction index between air and skin or glass and skin. As the Canny filter distorts the edges of an image, we removed the first and last two depth profiles before proceeding [Fig. 2(c)]. Then, the realignment was completed, and all B-scan profiles were shifted to the top of the image [Fig. 2(d)]. We maintained a height of 512 pixels for the  $z$  axis, assigning a value of zero to pixels where there was no information about the intensity because of the upshifting.

After the realignment, the intensity profile of Fig. 2(d) was averaged in time, producing plots similar to Fig. 2(e). We converted the pixel units to mm using the technical specifications of our OCT equipment (3 mm = 512 pixels) in the depth ( $z$ ) direction, which grows with skin penetration. To produce plots such as Fig. 2(e), the OCT pixel-size-to-length conversion rate was used, and the length (depth,  $z$ ) was corrected using a refractive index of 1.41 [20].

An intensity profile of the forearm [Fig. 2(e)] shows two peaks, caused by the two bright reflecting bands. The first peak is caused by the skin surface; this is defined as the depth at which the intensity of the first peak has reached half of its maximum. The second peak is caused by the reflection of dermal fibers [11,21–23]. The region up to 0.12 mm of depth in relation to the second peak maximum that corresponds to the papillary dermis layer was chosen for the analysis. That region has a linear characteristic and allows for a correspondence with the theoretical model for data regression and calculation of the attenuation coefficient in  $\text{mm}^{-1}$  [Fig. 2(e)].

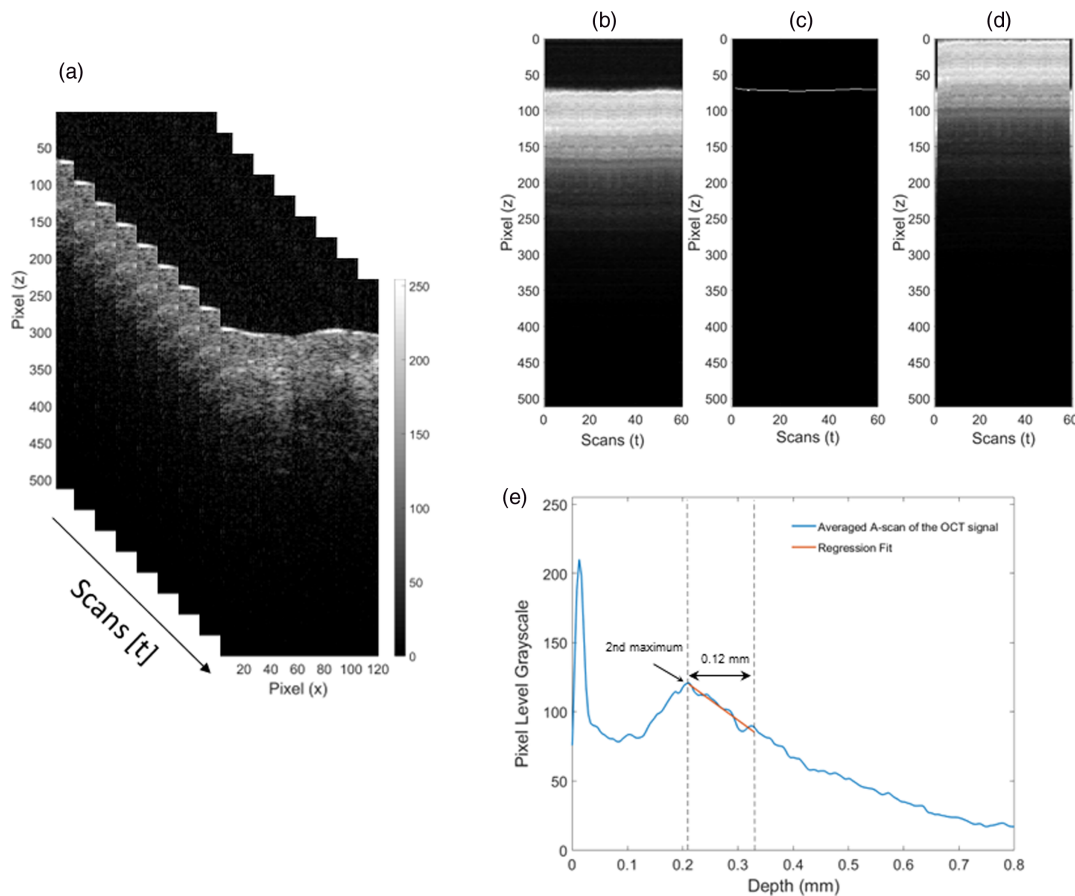


**Fig. 2.** Sequence of OCT image processing, where  $z$  represents depth coordinates and  $x$  represents axial coordinates. (a) Representation of some ROIs detached from B-scans. In the figure, only nine B-scans in time are shown in gray scale. (b) Image matrix built from intensity profiles computed from B-scans ROI shown in (a); each column represents one intensity profile. Note that the peaks of maximum intensity are not aligned. (c) Canny surface detection filter with the binary threshold (equal to 0.9). The white line indicates the pixels of maximum intensity obtained from (b). (d) Image matrix after the realignment procedure; as scans 1 and 59 are impaired in this process, it was necessary to remove the two initial and the two final scans. (e) Intensity profile, the average curve obtained from (d). The attenuation coefficient calculation in the dermis layer was performed from the second peak maximum up to 0.120 mm depth.

## 2. Step 2: Adjustment Method and Attenuation Coefficient Calculation

The intensity of backscattered light reaching the OCT detector decays exponentially with the depth. In this work, to explain the light attenuation in the skin, we adopt the single scattering model because of its simplicity and robustness in the description of the OCT signal at low optical depths [24,25],

$$I(z) = I_0 \cdot [\exp(-2 \cdot \mu_t \cdot z)]^{\frac{1}{2}}, \quad (1)$$

where  $I_0$  is the incident intensity,  $I(z)$  is the intensity of backscattered light at depth  $z$ , and  $\mu_t$  is the attenuation coefficient. The factor 2 in Eq. (1) is a consequence of round trip attenuation of light transport.

In the single scattering model, quantifying how the intensity of backscattered light  $I(z)$  is attenuated at a given depth ( $z$ ) implies determining the optical attenuation coefficient. A regression to the theoretical model was performed in the first region of the dermis, as already proposed by Su *et al.* [11]. The signal OCT images are given in gray scale (0 to 255). This gray scale represents the intensity of backscattered light, with

0 being the value with the lowest intensity (darkest) and 255 being the brightest white. The acquisition of OCT images was performed with a dynamic range of 50 dB empirically found to give better visual contrast between the true OCT signal and the background noise. By using the OCT manufacturer specification (see *Supplement 1*), a correction was made in Eq. (1) to determine the theoretical adjustment of the papillary dermis curve. We calculated  $\mu_t$  from the slope ( $A$ ) of a linear regression to the OCT signal in dB, which obeys  $I_{\text{dB}}(z) = -20 \log(e) \mu_t z$  (*Supplement 1*). However, the OCT signal is presented as pixel intensity, not as  $I_{\text{dB}}$ . The OCT dynamic range (50 dB) is presented as an 8-bit dynamic range (256 levels). This means that the intensity of a pixel corresponding to a zero intensity represents the OCT noise floor that is 50 dB below the signal represented by a pixel with an intensity of 255. Thus, a 50/255 scale transformation from OCT signals in dB to pixel levels is needed, and  $\mu_t$  is given by

$$\mu_t = \frac{A}{20 \log(e)} \cdot \frac{50}{255}, \quad (2)$$

where  $A$  is the slope of the linear regression to  $I_{\text{db}}(z)$ . The R-squared values of all linear regressions were above 0.94.

### 3. RESULTS AND DISCUSSION

Figure 3 shows how the attenuation coefficient ( $\mu_t$ ) varies as a function of the compression applied on the forearm of three volunteers (S1, S2, and S3). The attenuation coefficient for S1 ranged from 1.27 to 3.9  $\text{mm}^{-1}$  with a mean of  $2.65 \pm 0.83 \text{ mm}^{-1}$ ; for S2, it ranged from 1.27 to 3.50  $\text{mm}^{-1}$  with a mean of  $2.57 \pm 0.60 \text{ mm}^{-1}$ ; for S3, it ranged from 2.39 to 4.89  $\text{mm}^{-1}$  with a mean of  $3.32 \pm 0.78 \text{ mm}^{-1}$ . The data and code are provided in [Supplement 1](#).

Compared to  $\mu_t$  without any compression, a sharp decrease in optical attenuation is observed for skin compressions around 1 kPa ( $\sim 1/3$  reduction of  $\mu_t$ ). For higher compression values,  $\mu_t$  is a slowly decreasing function of compression. Our results in Fig. 3 indicate that, as compressions decrease to very low values ( $< 1 \text{ kPa}$ ), there is a sharp increase in the attenuation coefficient. The OCT-based observation agrees with what is observed by the naked eye when the skin becomes clearer under relatively low pressure, such as in capillary refill time (CRT) experiments [26]. Though the attenuation coefficient decreases as the compression increases, there are still small differences between the attenuation coefficient dependence with compression for different volunteers (Fig. 3). This physiological variability is expected and can be attributed to the intrinsic properties of the skin of each volunteer as skin color [27], sex [28], and natural hydration of the skin [21]. Similar behavior was reported by Chan *et al.* [29], who used diffuse reflectance to determine the optical properties of skin under a load of different human specimens. In this study, there was no control of specimens; thus, depending on volunteers, different values for attenuation coefficient were expected. In another study [30], it was demonstrated that soft tissues with very heterogeneous microstructure exhibit asymmetric tension/compression properties during elastic deformation;

consequently, the variability inter-volunteers with nonlinear-elastic properties of skin can modify its optical properties and show different values of attenuation coefficient.

The effect of compression on the optical properties of skin has been investigated in many previous studies. However, these studies typically have used compressions above 8 kPa [31,32] and have reported a decrease in the absorption coefficient and an increase in the scattering coefficient [33]. Furthermore, they have shown that there is an increase in the concentration and rearrangement of skin components, which leads to an increase in the contrast in OCT images, indicating an increase in the scattering coefficient. In contrast, our study found that, for compressions below 8 kPa, there was a decrease in the attenuation coefficient of the papillary dermis, with a minimum at around 1 kPa. This may be explained by the structure of the papillary dermis, which is composed of collagen fibrils, oxytalan elastic fibers, and finger-like projections called papillae that contain either terminal networks of blood capillaries or tactile corpuscles [34]. A reduction in extracellular liquid reduces the refractive index mismatch between the medium and cellular components, resulting in reduced scattering and increased contrast in OCT images. Thus, scattering is reduced, and light is directed to the OCT detector via backscattering, resulting in an increment in the contrast and penetration depth of OCT images. This technique is also known as tissue clearing [35].

The compression applied to the skin surface in this study is relatively low ( $< 8 \text{ kPa}$ ), less than the typical contact pressures felt at the fingertip by a finger oximeter [36]. However, 7 kPa is adequate for CRT tests [26], for example. Knowledge of an optimal compression range applied on the skin surface or other tissues is important because it allows for improving sensitivity and repeatability in OCT imaging, diffuse spectroscopy [37], and photobiomodulation [38].

Our results for the attenuation coefficients of forearms without compression ( $3.2 \text{ mm}^{-1}$  to  $4.9 \text{ mm}^{-1}$ ) compare well with the literature. For example, for the attenuation coefficients of forearms without compression measured well with 1300 nm OCT the literature reports values between  $2.9 \text{ mm}^{-1}$  and  $5.1 \text{ mm}^{-1}$  [25,39–41]. Our values are also close to the  $4 \text{ mm}^{-1}$  obtained in a previous study of ours [42] that used a similar protocol for  $\mu_t$  calculation. Yet, there are variations in the  $\mu_t$  values between participants (Fig. 3), which we believe to be due to the intrinsic characteristics of their skin, such as age, sex, natural hydration, and skin color [21,27,28]. The main contribution of our results to the literature is to provide  $\mu_t$  values for compression levels under 8 kPa.

To address concerns regarding skin stability during OCT scanning, we investigated potential spatial and temporal issues. To mitigate temporal fluctuations in skin-related properties, we opted to time-average the observation of the attenuation coefficient for 6 s. The possible sources of time instability we have identified are based on primary physiological mechanisms that may influence skin compression: (a) the heartbeat and (b) the respiratory cycle. Heartbeats subtly modulate the skin's optical properties, as demonstrated in our recent publication [42]. The respiratory cycle may induce involuntary movements of the forearm, which are also minimal. For example, in that study [42], we show the average value for an average attenuation coefficient of skin was  $4 \text{ mm}^{-1}$ , and the standard deviations due

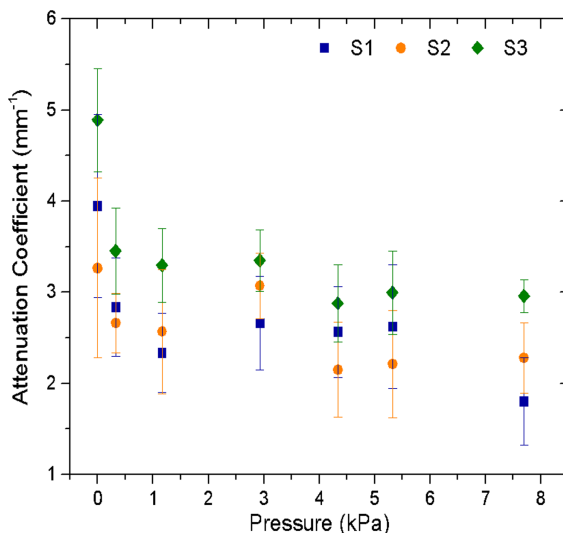


**Fig. 3.** Values of the attenuation coefficient of the papillary dermis layer of the forearm of three volunteers versus compression. The letters S1, S2, and S3 refer to three different subjects.

to the temporal and spatial variations were  $\sigma_T = 0.7 \text{ mm}^{-1}$  and  $\sigma_X = 0.3 \text{ mm}^{-1}$ , respectively, which evidentiate low noise during sample scanning.

This study has some limitations: (i) There was a low number of volunteers; furthermore, we used a sequence of 12 compressions, acquiring 56 A-scans for each compression, in total 672 A-scans for each volunteer. (ii) It was not possible to accurately estimate the pressure uncertainty, so in Fig. 3 there is no pressure uncertainty bar. (iii) The compression time was around 1 min. It is known that optical clearance is a function of the time the compression has been applied to the skin [35]. The results shown in this work were performed only for the first layer (papillary dermis) of the dermis; thus, we are not aware of the behavior in the deep region of the dermis due to a poor signal-to-noise ratio.

Finally, we will consider future work with an increased number of subjects for the study, investigating how elasticity may be influencing the results. We suggest that, by measurement or by inspection, it might be possible to find an optimum low compression for each individual for biomedical optical interventions.

#### 4. CONCLUSION

In this study, we investigated how low mechanical compression modifies the value of the attenuation coefficient of skin. The average depth profiles obtained from OCT B-scans were analyzed using the Beer–Lambert equation, which describes the propagation of light in biological tissues. Our results show that applying low levels of compression to the skin decreases its attenuation coefficient, which in turn may improve the delivery of light to deeper tissues. Inter-individual variations were found to be small, and the overall behavior was found for all three volunteers. Low compression used to reduce the optical attenuation coefficient of skin may improve non-invasive imaging diagnosis, therapies and treatments, and experimental studies.

**Funding.** Coordenação de Aperfeiçoamento de Pessoal de Nível Superior (001).

**Acknowledgment.** The authors gratefully acknowledge Prof. Jean Pierre von der Weid and Centro de Estudos em Telecomunicações (CETUC) of Pontifícia Universidade Católica do Rio de Janeiro and Prof. Luciano Bachmann for providing OCT equipment and software. This study was financed by the Coordenação de Aperfeiçoamento de Pessoal de Nível Superior—Brazil (CAPES). R. P. participated in data collection, performed the analytic calculations, performed the numerical simulations, and wrote the first version of the paper. C. T. D. helped to design the experiment, collected the data, contributed to the analysis of the data, and helped to write the paper with input from all authors. G. C. C. conceived the original idea. All the authors discussed the results and commented on the paper. All authors read and approved the final paper.

**Disclosures.** Ethical approval for this study was obtained from the University of São Paulo Ethics Committee CAAE 95342518.1.0000.5407, 3.046.098/FFCLRP. The investigation conformed to the principles in the Declaration of Helsinki (World Medical Association 2000); all subjects were included voluntarily and gave their written informed consent. The data produced for this paper are available at [43].

**Data availability.** Data underlying the results presented in this paper are not publicly available at this time but may be obtained from the authors upon reasonable request.

**Supplemental document.** See Supplement 1 for supporting content.

#### REFERENCES

1. M. Hohmann, M. Späth, D. Ni, D. Dörner, B. Lengenfelder, F. Klämpfl, and M. Schmidt, “Random laser as a potential tool for the determination of the scattering coefficient,” *Biomed. Opt. Express* **12**, 5439–5451 (2021).
2. C. G. Rylander, T. E. Milner, S. A. Baranov, and J. S. Nelson, “Mechanical tissue optical clearing devices: enhancement of light penetration in ex vivo porcine skin and adipose tissue,” *Lasers Surg. Med.* **40**, 688–694 (2008).
3. P. Gong, M. Almasian, G. van Soest, D. M. de Bruin, T. G. van Leeuwen, D. D. Sampson, and D. J. Faber, “Parametric imaging of attenuation by optical coherence tomography: review of models, methods, and clinical translation,” *J. Biomed. Opt.* **25**, 040901 (2020).
4. D. Pal, S. Agadarov, Y. Beiderman, Y. Beiderman, A. Kumar, and Z. Zalevsky, “Non-invasive blood glucose sensing by machine learning of optic fiber-based speckle pattern variation,” *J. Biomed. Opt.* **27**, 097001 (2022).
5. R. He, “Effects of optical clearing agents on noninvasive blood glucose monitoring with optical coherence tomography: a pilot study,” *J. Biomed. Opt.* **17**, 101513 (2012).
6. G. Gunaydin, M. E. Gedik, and S. Ayan, “Photodynamic therapy—current limitations and novel approaches,” *Front. Chem.* **9**, 691697 (2021).
7. S. Rajesh, E. Koshi, K. Philip, and A. Mohan, “Antimicrobial photodynamic therapy: an overview,” *J. Indian Soc. Periodontol.* **15**, 323–327 (2011).
8. V. V. Tuchin, E. A. Genina, E. S. Tuchina, A. V. Svetlakova, and Y. I. Svenskaya, “Optical clearing of tissues: issues of antimicrobial phototherapy and drug delivery,” *Adv. Drug Deliv. Rev.* **180**, 114037 (2022).
9. C. G. Rylander, A. A. Gurjarpadhye, W. C. Vogt, and Y. Liu, “Effect of localized mechanical indentation on skin water content evaluated using OCT,” *Int. J. Biomed. Imaging* **2011**, 817250 (2011).
10. M. Y. Kirillin, P. D. Agrba, and V. A. Kamensky, “In vivo study of the effect of mechanical compression on formation of OCT images of human skin,” *J. Biophoton.* **3**, 752–758 (2010).
11. Y. Su, X. S. Yao, C. Wei, Y. Wang, H. Wang, and Z. Li, “Determination of the pressure coefficient of optical attenuation in different layers of in-vivo human skins with optical coherence tomography,” *IEEE Photon. J.* **8**, 3800110 (2016).
12. A. A. Kamshilin, O. V. Mamontov, V. T. Koval, G. A. Zayats, and R. V. Romashko, “Influence of a skin status on the light interaction with dermis,” *Biomed. Opt. Express* **6**, 4326–4334 (2015).
13. J. A. Delgado Atencio, E. E. Orozco Guillén, S. Vázquez y Montiel, M. C. Rodríguez, J. C. Ramos, J. L. Gutiérrez, and F. Martínez, “Influence of probe pressure on human skin diffuse reflectance spectroscopy measurements,” *Opt. Mem. Neural Netw.* **18**, 6–14 (2009).
14. D. R. T. Sampaio, C. R. Albino, R. G. Palma-Dibb, P. Jean, P. Von Der Weid, L. Bachmann, and C. T. Dominguez, “Optical attenuation coefficients of moist and dry tooth determinate by optical coherence tomography,” *Braz. J. Phys.* **52**, 209 (2022).
15. A. I. Kholodnykh, I. Y. Petrova, M. Motamedi, and R. O. Esenaliev, “Accurate measurement of total attenuation coefficient of thin tissue with optical coherence tomography,” *IEEE J. Sel. Top. Quantum Electron.* **9**, 210–221 (2003).
16. P. Lee, W. Gao, and X. Zhang, “Performance of single-scattering model versus multiple-scattering model in the determination of optical properties of biological tissue with optical coherence tomography,” *Appl. Opt.* **49**, 3538–3544 (2010).
17. S. Mine, N. O. Fortunel, H. Pageon, and D. Asselineau, “Aging alters functionally human dermal papillary fibroblasts but not reticular fibroblasts: a new view of skin morphogenesis and aging,” *PLoS One* **3**, e4066 (2008).
18. J. Canny, “A computational approach to edge detection,” *IEEE Trans. Pattern Anal. Mach. Intell.* **PAMI-8**, 679–698 (1986).

19. A. Hojjatoleslami and M. R. N. Avanaki, "OCT skin image enhancement through attenuation compensation," *Appl. Opt.* **51**, 4927–4935 (2012).
20. G. J. Tearney, M. E. Brezinski, B. E. Bouma, M. R. Hee, J. F. Southern, and J. G. Fujimoto, "Determination of the refractive index of highly scattering human tissue by optical coherence tomography," *Opt. Lett.* **20**, 2258–2260 (1995).
21. F. M. Hendriks, D. Brokken, C. W. J. Oomens, and F. P. T. Baaijens, "Influence of hydration and experimental length scale on the mechanical response of human skin *in vivo*, using optical coherence tomography," *Skin Res. Technol.* **10**, 231–241 (2004).
22. J. Welzel, E. Lankenau, R. Birngruber, and R. Engelhardt, "Optical coherence tomography of the human skin," *J. Am. Acad. Dermatol.* **37**, 958–963 (1997).
23. Y. Hori, Y. Yasuno, S. Sakai, M. Matsumoto, T. Sugawara, V. D. Madjarova, M. Yamanari, S. Makita, T. Yasui, T. Araki, M. Itoh, and T. Yatagai, "Automatic characterization and segmentation of human skin using three-dimensional optical coherence tomography," *Opt. Express* **14**, 1862–1877 (2006).
24. L. Scolaro, R. A. McLaughlin, B. R. Klyen, B. A. Wood, P. D. Robbins, C. M. Saunders, S. L. Jacques, and D. D. Sampson, "Parametric imaging of the local attenuation coefficient in human axillary lymph nodes assessed using optical coherence tomography," *Biomed. Opt. Express* **3**, 366–379 (2012).
25. P. Gong, "Assessment of human burn scars with optical coherence tomography by imaging the attenuation coefficient of tissue after vascular masking," *J. Biomed. Opt.* **19**, 021111 (2013).
26. R. P. de Souza and G. C. Cardoso, "Skin color independent robust assessment of capillary refill time," *arXiv*, arXiv:2102.13611 (2021).
27. A. Alex, B. Považay, B. Hofer, S. Popov, C. Glittenberg, S. Binder, and W. Drexler, "Multispectral *in vivo* three-dimensional optical coherence tomography of human skin," *J. Biomed. Opt.* **15**, 026025 (2010).
28. F. Auriol, L. Vaillant, L. Machet, S. Diridollou, and G. Lorette, "Effects of short time hydration on skin," *Acta Derm Venereol.* **73**, 344–347 (1993).
29. E. K. Chan, B. Sorg, D. Protsenko, M. O'Neil, M. Motamedi, and A. J. Welch, "Effects of compression on soft tissue optical properties," *IEEE J. Sel. Top. Quantum Electron.* **2**, 943–950 (1996).
30. J. Z. Wu, R. G. Cutlip, M. E. Andrew, and R. G. Dong, "Simultaneous determination of the nonlinear-elastic properties of skin and subcutaneous tissue in unconfined compression tests," *Skin Res. Technol.* **13**, 34–42 (2007).
31. O. A. Zyuryukina and Y. P. Sinichkin, "The dynamics of optical and physiological characteristics of human skin *in vivo* during its compression," *Opt. Spectrosc.* **127**, 555–563 (2019).
32. I. A. Nakhaeva, M. R. Mohammed, O. A. Zyuryukina, and Y. P. Sinichkin, "The effect of an external mechanical compression on *in vivo* optical properties of human skin," *Opt. Spectrosc.* **117**, 506–512 (2014) (English Transl. Opt. i Spektrosk.).
33. L. Lim, B. Nichols, N. Rajaram, and J. W. Tunnell, "Probe pressure effects on human skin diffuse reflectance and fluorescence spectroscopy measurements," *J. Biomed. Opt.* **16**, 011012 (2011).
34. M. Keck, D. B. Lumenta, and L. P. Kamolz, "Skin tissue engineering," in *Dermal Replacements in General, Burn, and Plastic Surgery: Tissue Engineering in Clinical Practice* (Elsevier, 2014), pp. 13–25.
35. T. Tian, Z. Yang, and X. Li, "Tissue clearing technique: recent progress and biomedical applications," *J. Anat.* **238**, 489–507 (2021).
36. Y. Nagashima, Y. Yada, M. Hattori, and A. Sakai, "Development of a new instrument to measure oxygen saturation and total hemoglobin volume in local skin by near-infrared spectroscopy and its clinical application," *Int. J. Biometeorol.* **44**, 11–19 (2000).
37. C. Li, J. Jiang, and K. Xu, "The variations of water in human tissue under certain compression: studied with diffuse reflectance spectroscopy," *J. Innov. Opt. Health Sci.* **6**, 1350005 (2013).
38. A. Gobbi, G. de Carvalho, A. T. Sapalo, and R. R. de Jesus Guiro, "Acute application of photobiomodulation does not bring important gains for the muscular performance and functionality of diabetic individuals," *Laser Med. Sci.* **36**, 995–1002 (2021).
39. J. M. Schmitt, A. Knüttel, and R. F. Bonner, "Measurement of optical properties of biological tissues by low-coherence reflectometry," *Appl. Opt.* **32**, 6032–6042 (1993).
40. J. Welzel, M. Bruhns, and H. H. Wolff, "Optical coherence tomography in contact dermatitis and psoriasis," *Arch. Dermatol. Res.* **295**, 50–55 (2003).
41. S. Es'haghian, P. Gong, L. Chin, K. A. Harms, A. Murray, S. Rea, B. F. Kennedy, F. M. Wood, D. D. Sampson, and R. A. McLaughlin, "Investigation of optical attenuation imaging using optical coherence tomography for monitoring of scars undergoing fractional laser treatment," *J. Biophoton.* **10**, 511–522 (2017).
42. C. T. Dominguez, M. B. Martinelli, L. Bachmann, and G. C. Cardoso, "Arterial pulsation modulates the optical attenuation coefficient of skin," *J. Opt. Soc. Am. A* **40**, C87–C92 (2023).
43. Photobiomedical Instrumentation Group, "AttCoefOCT," GitHub (2022), <https://github.com/Photobiomedical-Instrumentation-Group/AttCoefOCT>.